Performance of GPS-TEC assisted NTCM-model to describe the East-African equatorial Ionosphere

B. Getahun[1], M.Nigussie [1]

[1]Washera Geospace and Radar Science Laboratory, Bahir Dar University, Bahir Dar, Ethiopia

Abstract

NTCM is a simple and relatively faster global climatological model that is developed, using ionospheric VTEC measurements from unevenly globally distributed GNSS receivers, to mitigate ionospheric effects on GNSS applications. As it is climatological, its ionospheric weather characteristic specification capability is limited. Also, its nowcasting and forecasting performance in the East-African equatorial ionosphere has not yet been tested. Therefore, this paper demonstrates techniques to change NTCM to ionospheric weather model to nowcast and forecast VTEC for East-Africa. NTCM has been changed to ionospheric weather model through adapting it to quiet days VTEC from nineteen GNSS receivers in East-Africa in 2013 and 2014. Adaptation has been done by calculating its driver, effective ionization level, when NTCM modeled VTEC fits the best with observed VTEC. Then, performances of the model in nowcasting and forecasting VTEC, before and after adaption, have been investigated compared to observed VTEC. It is found that NTCM, after adaptation, represents observed features of diurnal variations of VTEC and equatorial ionization anomaly (EIA) much better than before adaptation. After adaptation, the mean and standard deviation of daily mismodelings are found comparable with the mean and standard deviation of yearly mismodelings. It is demonstrated also that NTCM after adaptation to a reference station performs better than before adaptation at the stations nearby the reference station; however, its performance decreases at the locations far away from the reference station. In addition, after adaptation, one hour ahead prediction of NTCM is found to be the best compared to its longer hours prediction.

Key words: data ingestion, NTCM-model, model performance.

Key points: 1) The diurnal performance of NTCM is found to be improved by data ingestion. 2) Spatial performance of NTCM has become better after adaptation.3) Model VTEC map run by Az reflects the observations such as EIA.

Corresponding Authors: Balew Getahun (balewwgetahun@gmaill.com) & Melessew Nigussie (melessewnigussie@yahoo.com)

Introduction

Ionosphere is the region of Earth's atmosphere which contains significant amount of free electrons and ions (*Schunk and Nagey,* 2009). The primarily source of the ions and free electrons is photoionization of solar radiation. Ionosphere is approximately located in altitude range between 50 kms and higher than 2000 kms above sea level. The level of significance of number of ions and electrons found in the atmosphere is determined by the effect that the atmosphere acts on the radio signals when it attempts to pass through (*Davies,* 1990, Zolesi. et al., 2014). Ionosphere is mainly characterized by its electron density (Ne) or total electron content (TEC) of a column of unit base area extended between the Global Positioning System (GPS) satellite and receiver along the signal path. Ionosphere is taken as both resource and setback for some of the modern technologies. In case of satellite based navigation, it degrades performance by introducing extra delay (slowing down and bending propagation) and/or scintillation of radio signals used by GPS. Error in GPS navigation caused by ionosphere is the most significant (Tiwari et al., 2013, *Davies,* 1990). However, in radio communication, radio signals are reflected by the bottom side of the ionosphere thus ionosphere helps radio transmission over the horizon (Rawer, 1993).

After extensive studies for more than five decades, it is well known that the "climate" change and "weather" disturbance of ionosphere are caused by processes extended from ionosphere-thermosphere system to mesosphere, solar, interplanetary and magnetosphere dynamics (Schunk et al., 2004). The ionosphere characteristics depend on location, season, time of the day, and solar activity level (Jakowski et al., 2011; Scherliess et al., 2008).

The ionosphere variability affects radio signal propagation adversely. However, it is possible to mitigate this effect if we specify and predict spatiotemporal dynamics of the ionosphere. This can be possible through developing a model that characterizes ionosphere. Empirical models such as International Reference Ionosphere (IRI) (Bilitza et al., 2018), NeQuick-2 (Nava et al., 2008), and Neustrelitz TEC model (NTCM) (Jakowski et al., 2011) have been developed to specify the climatological ionosphere behavior.

In specifying peak electron density, IRI and NeQuick models perform well, however they take longer time and lack accuracy in estimating TEC. Measuring their shape parameters is difficult, and inaccuracy of modeling the topside ionosphere and plasmasphere morphology results in crucial errors in estimating TEC (Jakowski et al., 2011). To calculate TEC, IRI and NeQuick models integrate Ne numerically along the line joining two points in space.

However, NTCM model is another empirical model which estimates VTEC directly. It takes shorter time to compute TEC since it doesn't need to integrate Ne. NTCM works for all solar activity levels taking F10.7 as the main driving parameter and it uses only 12 model coefficients (Jakowski et al., 2011). These empirical models represent the monthly median value of the ionosphere Ne or TEC. They lack capability of reproducing the current ionosphere conditions (Bilitza et al., 2008; Nava et al., 2011; Jakowski et al., 2011).

In order to a model can capture short-time variations, we use either data assimilation or data ingestion technique (Ercha et al., 2018; Nava et al., 2011; Brunini et al.,2011). In case of data assimilation, we use measurements and optimization algorithms like Kalman filter to determine the initial and boundary conditions of ionosphere physical models. Global Assimilation Ionosphere models (GAIM), for example, used different sources of ionosphere data like ground and space based GPS measurements, Ionosonde-derived electron density profiles, UV airglow, in situ electron and neutral densities, plasma drift, neutral wind measurements to create "weather" prediction model (Wang et al., 2004). Another example of data assimilative model is Electron Density Assimilative Model (EDAM) (Angling and Jackson-Booth, 2011*).* EDAM used different ionosphere data sources such as TEC-data taken from both ground and space based GNSS receivers and electron density profiles obtained from ionosondes, incoherent scattering radars, and in situ measurements in order to effectively specify nearly real–time characteristics of the ionosphere with minimal errors in both TEC and *fo*F2. However, due to its simplicity and less computation time, data ingestion into empirical models attracts more of space weather communities (Ercha et al., 2018). Data ingestion uses the application of simple minimization algorithms like least square to force a parameterized empirical model to capture nearly the current behavior of the ionosphere. One of the parameters of the model represents level of ionization which is known as effective ionization level (Az). The purpose of data ingestion is to determine Az that minimizes the deviation of the model from the observation.

Number of studies showed that data ingestion into NeQuick model has improved its performance. Nava et al. (2006) has applied data ingestion to NeQuick model using single and multiple GPS receivers and showed that in both cases near real-time ionosphere characteristics are retrieved. Moreover, the capability of TEC reconstruction in case of multiple stations is more remarkable than single station due to higher data density. Brunini et al. (2011) have applied data ingestion into NeQuick2 model and found that the model error could be reduced to 25-30% for slant TEC (STEC) and Ne. Olwendo et al. (2016) applied the

ingestion for NeQuick2 model using GPS data over the Kenyan regions and was able to show that the difference between the measured and model TEC is minimized to the value of 0.5 TECU. Nigussie et al. (2012) also used data ingestion into NeQuick2 model using GPS data over Easter Africa ionosphere and showed that the performance of the model after data ingestion at a reference station is substantially improved for stations located up to 620 kms from the reference station. Ercha et al. (2018) used data ingestion for NeQuick2 model in combination with Empirical Orthogonal Function (EOF) analysis and reached to a result 10–15% improvement of accuracy over the standard ionosphere correction algorithm in the Galileo navigation system.

IRI and NeQuick models use smoothed monthly mean sun spot number (Rz_{12}) or F10.7 which are related by (M. G. Deminov and G.F Deminova, 2018, Rec. ITU-R P.371-8)

$$F_{12} = 63.7 + 0.78Rz_{12} + 8.9x10^{-4}Rz_{12}^{2} \ , \quad (1)$$

where F_{12} is monthly mean of F10.7.

Equation 1 implies that to get positive sun spot number, there is a constraint on values of F10.7 flux that it has to be greater than 63.7 Solar Flux Unite (SFU) as recommended by ITUR (1997). The mathematical function used in NTCM and IRI (NeQuick) are different and hence it will have difference on application of data ingestion in these families of empirical models. When we apply data ingestion into IRI and NeQuick models, the Az value might be less than 63.7 SFU, as shown for example in Nigussie et al.(2016) against ITUR (ITU-R P.371-8) recommendation, and that will be used in the models internally to compute negative sunspot number which is unrealistic. This might be resolved when we apply data ingestion to NTCM model, since the mathematical formulation for NTCM is different from IRI and NeQuick2.

In this study, we focus on the investigation of NTCM model performance in the East African equatorial ionosphere by assisting it with GPS vertical TEC (VTEC) data applying ingestion technique. First GPS-VTEC data is ingested to the model to determine the optimal Az then the performance of the model in reconstructing VTEC using Az is tested. To test the spatial performance of adapted model, the Az computed at one particular (reference) station is used for different stations. Some statistical analysis is also made for the comparison of the mis-modeling level in reproducing VTEC before and after ingestion.

2. Data and the Analysis Method

2.1 Model

NTCM model has been developed by Jakowski et al. (2011) at DLR Neustrelitz Germany. It is an empirical model with few model coefficients (only 12). The model consists of five major independent functions. The functions depend on location (latitude and longitude), time (diurnal and seasonal) and solar activity. The solar activity is represented by the daily solar flux index F10.7. The output of NTCM is VTEC of ionosphere of region of interest. The details and full mathematical expressions of the model are found in Jakowski *et al. (2011).* NTCM model is simplified but it doesn't capture the real-time variation of VTEC. To use the model for weather variation, we have to adapt it to ionosphere sector of interest at a given time (local time, day, month or season).

2.2 Data ingestion

As NTCM is regarded a monotonic function of F10.7, it is assumed that NTCM is a local ionization driven model. The local ionization level that plays the role of effective solar flux index in estimating VTEC of the model at a given Ionosphere pierce point (IPP) and in an epoch of time is Az. As many literatures reviewed (Nigussie et al., 2012, Ercha et al., 2018, Nava et al., 2006), Az is determined by minimizing the root mean square error (RMSE) defined in equation 2.

$$\mathrm{RMSE(Az)} = \sqrt{\frac{\sum_{i}^{N}(\mathrm{VTECm_i(Az)} - \mathrm{VTECo_i})^2}{N}}, \quad (2)$$

where, $\mathrm{VTECm_i(Az)}$ is the model VTEC computed as function of Az , $\mathrm{VTECo_i}$ is measured VTEC, and N is the number of satellites visible in an epoch of time.

To determine Az, NTCM is driven by a range of F10.7 values then the one which minimizes equation (2) for each hour of measurements is chosen. The chosen values will be Az in the hours of the day. Then the model VTEC after data ingestion is calculated using Az whereas before ingestion VTEC is computed using daily average F10.7. To test the spatial performance of the model after adaptation, we run the model using Az computed at one (reference) station to other stations.

2.3 Vertical TEC mapping Techniques

NTCM has been also used to develop map of VTEC before and after data ingestion for East African region. Nineteen GPS stations (see Table 1 for their coordinates) have been used to develop VTEC maps after data ingestion. First Az values have been estimated at each IPP for every hour using equation (2), then Az values in IPP plan is represented by the quadratic function that varies in latitude and longitude. The polynomial used is formulated from linear variation in longitude (λ) and quadratic variation in latitude (θ), and it is expressed by

$$Az\ (\vartheta, \lambda) = a_0 + a_1\vartheta + a_2\lambda + a_3\lambda\vartheta + a_4\vartheta^2 \qquad (3)$$

where, the a's are coefficients of the polynomial and they are estimated from the Az values applying the least-square fitting technique. Once the coefficients are estimated, equation (3) has been used to estimate the map of Az that has been used to drive NTCM to estimate the map of VTEC after data ingestion. Similarly, equation (2) has been also fitted directly to VTEC observation and then the equation has been used to estimate VTEC at any latitude and longitude to produce VTEC map. The corresponding map of VTEC before adaption has been estimated by running NTCM in the same region using daily F10.7 values as model driver. The performance of the model in estimating VTEC map before and after adaptation has been compared with the VTEC maps estimated directly from the quadratic equation (3) and observed VTEC.

2.4 Data

These days GPS data over African sector are easily accessible due to ground based receivers deployed in the continent. For example in Ethiopia there are numbers of GPS receiver stations (www.unavco.org). These opportunities have laid a good platform for studying the region's ionosphere dynamics. Using these data many global models are under investigation for their validity of performance (Nigussie et al., 2012; Nigusie et al., 2016; Tariku et al., 2015; Olwendo et al., 2016).

For this particular study, we chose nineteen sample sites in East Africa. The geographic and geomagnetic locations of the sites are shown in Table 1. We considered data of magnetic quiet time in the years 2014 and 2013 so the study is limited for quiet conditions. Days of year (DOYs) with Ap greater than 20 are excluded. The reason taken to choose the sites is

availability of relatively full data for the four seasons of the year (Jun solstice, September equinox, December solstice and March equinox).

Table 1: geographic and geomagnetic location of the GPS stations

Stations	Code	Geographic		Geomagnetic		Dip –latitude
		Latitude (^{o}N)	Longitude (^{o}E)	Latitude (^{o}N)	Longitude (^{o}E)	
Bahir Dar	BDMT	11.60	37.36	8.07	111.48	3.63
Ambo	ABOO	8.99	37.81	5.44	111.50	0.78
Assosa	ASOS	10.05	34.55	7.00	108.48	1.50
Addis Ababa	ADIS	9.05	38.77	5.39	112.44	0.98
Arba Minch	ARMI	6.06	37.56	2.63	110.78	-2.53
Asab	ASAB	13.06	42.65	8.75	116.86	5.93
Asum	ASUM	-0.62	34.62	-3.49	106.82	-10.34
Debark	DEBK	13.15	37.89	9.58	112.24	5.44
Ginir	GINR	7.15	40.71	3.21	114.05	-0.88
Malindi	MAL2	-3.00	40.19	-6.74	111.96	-12.16
Mbarara	MBRA	-0.60	30.74	-2.83	102.99	-10.89
Eldoret	MOIU	0.29	35.29	-2.70	107.63	-9.24
Nazret	NAZR	8.57	39.29	5.01	112.9	-0.51
Negele	NEGE	5.33	39.59	1.59	12.66	-3.06
Nirobi	RCMN	-1.22	36.89	-4.45	108.97	-10.67
Robe	ROBE	7.11	40.03	3.7	113.37	-1.02
Seraba	SERB	12.51	37.02	9.08	111.28	4.61
Shimsheha	SHIS	11.99	38.99	8.26	113.12	4.29
Sheb	SHEB	15.85	39.05	12.06	113.81	8.60

The GPS RINEX data taken from UNAVCO website have been calibrated according to the techniques discussed in Ciraolo et al. (2007). The VTEC has been computed from calibrated STEC using the mapping function described in *Mannucci et* al. (1998). VTEC data of elevation angle less than 20^o were not included in order to reduce multipath effects.

The performances of the model (before and after ingestion) are determined by taking the difference of observed and modeled VTECs. Mis-modeling of the model is defined to be the difference between the measured and modeled value of ionosphere parameter at a location and in an epoch where data was taken. The level of mis-modeling determines the performance of the model. If the mis-modeling is high the performance of the model is low. If the mis-modeling is low the performance of the model becomes high. So to evaluate the effectiveness of the method we make a comparison of the model performance before and after data ingestion into the model.

3. Results and discussion

3.1 Day -to -day variation of performance of NTCM

Panels (a-d) of Figure 1 show the diurnal variations of observed (*red) and modeled VTEC before (black) and after (blue) adaptation at Ambo station for the DOYs 79, 171, 263 and, 355 in the year 2014. As we can see from the graphs, the model (before and after adaptation) generally captures the pattern of diurnal variation of observed VTEC throughout hours of the days. However, the model before adaptation reproduces observation VTEC for only small portion of the hours of the days. For larger portion of hours of the days, it generally overestimates VTEC as compared to the observation. For example, panel 'a' (DOY 79) , Panel 'b' (DOY 171) and panel 'c' (DOY 263) show that the model before adaptation captures observed VTEC from about 5 to 10 UTCs and for the rest hours of the days it overestimates. As shown in panel 'd' (DOY 355), the model before adaptation reproduces the observed VTEC approximately from about 5 to 8 UTCs. However, after adaptation the capability of the model to capture diurnal variations of VTEC is greatly improved. It retrieves the observation VTEC for almost all hours of the days considered.

The frequency distribution of mismodeling after and before adaptation for Ambo station is depicted in the middle and right panels of Figure 1, respectively. Each row panel depicts for different DOYs. The means (μ) and standard deviations (δ) are also included in the corresponding panels. The means of mismodeling before data ingestion in general are larger than their corresponding means of mismodeling after data ingestion. As seen from Figure 1, the mean before adaptation ranges from -5 to -26 TECU. However, the means after ingestion are from -0.030 to 0.04 TECU. The negative sign of means indicates that the model averagely overestimated the observation. The standard deviations of mismodeling after ingestion have

also decreased as compare to their values before ingestion. The standard deviations after ingestion for the DOY 79,171,263 and 355 are 3.92, 1.56, 3.51 and 3.91 TECU, respectively. The corresponding mismodeling standard deviations before adaptation are 14.54, 5.29, 11.23 and 17.85 TECU.

Figure 2 shows the same results as in Figure 1 but for Bahir Dar Station. Panels (a-d) in Figure 2 present the graphs of the modeled VTEC before (black) & after (blue) adaptation, and the observed (*red) VTEC versus hours of the selected days. Before adaptation, the capability of the model in retrieving VTEC seems poor. It only captures the trend of diurnal variation. However after adaptation, its capability is improved. In Figure 2, it is seen that the model (after adaptation) VTEC is more approximated to the observation VTEC. The middle and the right panels of Figure 2 present the frequency distributions of mismodeling before and after ingestion, respectively. The means and standard deviations of the mismodeling are included in the corresponding histograms of the distributions. Generally the means of mismodeling after adaptation are lower than that of before adaptation.

The mean after adaptation ranges from -0.02 to 0.02 TECU but it ranges from -5.66 to -21.42 TECU before adaptation. The standard deviations of mismodeling after adaptation are significantly decreased as compared to their corresponding values before ingestion. The range of standard deviations after adaptation is 1.57 to 5.78 TECU. But the standard deviation before adaptation varies from 5.11 to15.83 TECU. The reduction of means and standard deviations of mismodeling after adaptation indicates that the technique of ingestion has assisted the model to retrieve the observation better.

The same data ingestion technique has been applied for GPS data taken from Addis Ababa (Ethiopia), Malindi (Kenya), Mbarara (Uganda) and Asab (Eretria) stations. Figure 3-6 show results for these stations, respectively. Panels (a-b) in these figures indicate that the modeled VTEC after adaptation are in better agreement to experimental than the modeled VTEC before adaptation. The frequency distribution of mismodeling after ingestion is almost symmetric about 0 TECU. But in case of model before adaptation, the frequency distributions of the mismodeling are not as such much Gaussian. The means and standard deviations presented in Figure 3-6 panels (middle after adaptation and right before adaptation) quantify the performance of the model. The means and standard deviations of mismodeling have been significantly reduced by data ingestion as compared to their values of standard model. The

model before adaptation, in all the mentioned stations averagely overestimated the experimental VTEC.

In order to complement the results shown in Figures 1-6, we applied data ingestion for quiet 354 days in 2014 at Ambo station. Figure 7 presents frequency distribution of mismodelings before and after adaptation. As seen from the plots, the mean value before adaptation is -6.71 TECU but it is approximated to 0.01 TECU after adaptation. On average the model before adaptation overestimated the experimental values. The standard deviation is decreased from 14.56 to 3.34 TECU due to ingestion. In addition, the frequency distribution becomes more symmetric to 0 TECU after adaptation than before adaptation. In general, yearly mean and standard deviation of the mismodeling shown in Figure 7 are similar to the daily mean and standard deviations shown in the Figures 1-6. Therefore, the results shown above indicate that data ingestion assists NTCM model to capture the daily variability of VTEC.

3.2 Spatial Performance of NTCM after and before adaptation

To validate spatial performance of NTCM model after ingestion, we first ingested VTEC at Addis Ababa (reference) station to compute Az's. Then we tested its performance at stations Ambo, Bahir Dar, Assab and Nazret. The diurnal variations of both modeled and observed VTEC and mismodelings after and before ingestions for these stations respectively are shown in Figures 8, 9, 10, 11 for the DOY 79,171,263, and 355 in the year 2014. Figures 8-11, (a-b) panels present the diurnal variation observed (red) and modeled VTEC,- after (blue) and before (black) ingestion. The trends of retrieving the observed VTEC before and after adaptation are similar to results discussed in section 3.1. The modeled VTEC after adaptation is in better agreement with the observed VTEC than before adaptation. In the above mentioned figures, the mismodeling frequency distributions (the middle panels are after, and right are before adaptation) are included with their corresponding means and standard deviations. As seen, the means and standard deviations after adaptation have significantly decreased as compared to the corresponding values before adaptation. For example, the mean of mismodeling after adaptation for DOY 79 at Ambo is -5.79 TECU, whereas before adaptation, it is -20.29 TECU, and the standard deviation after adaptation is 5.07 TECU and before adaptation is 14.54 TECU. Similar improvement in the performance of NTCM has been observed at the other stations using Az from reference station as NTCM driver (see

Figures 9, 10, and 11). These indicate that NTCM adapted to a reference station performs better at other nearby stations compared to its performance before adaptation. However, the spatial performance decreases as the distance between a station and a reference (Addis Ababa) increases. The air distances between Addis Ababa, and Bahir Dar, Nazret, Ambo and Assab are around 324, 79, 98, and 620 km, respectively. For example, the performance of the model at Nazerte (nearest) station (see Figure 11) is by far better than at Assab (farthest) station (see Figure 10).

3.3 Prediction capability of NTCM after adaptation

For operational application, a model performance ahead of time is very essential. As a test study, 1hr, 2hrs, 3hrs and 4hrs prediction capability of NTCM have been investigated. For example, Az obtained at previous hour has been used to drive NTCM to predict VTEC at the present hour; and the comparison between predicted and observed VTEC at the present hour indicates one hour ahead prediction capability of the model. Figure 12 shows the diurnal variation of measured, modeled (before & after ingestion) and predicted VTEC at Ambo station for DOY 355 in 2014. As seen in the figure, the prediction capability of the model decreases, as the length duration of computing Az increases. The gap between the predicted VTEC and measured VTEC for 1hr ahead prediction is small as compared to for 4hrs ahead prediction. So the performance of the model gets weaker when the prediction time is elongated.

3.4 Vertical TEC map after and before adapting NTCM

Data taken from 19 stations on DOY 110 in the year 2013 have been used to develop VTEC maps. NTCM modeled VTEC maps before and after adaptation have been developed by driving the model using F10.7 and Az maps, respectively. Also, VTEC maps have been developed by representing observed VTEC using quadratic polynomial function. Samples maps were developed on DOY 110 in 2013 at 2, 4, 6,8,10,12,14,16 and 18 UTCs. Figures 13 and 14 show the scatter (left column) and contour map (2^{nd}, 3^{rd} and 4^{th} column from the left) plots of observed and modeled VTEC, respectively. Each row panels, from top to bottom, in these figures respectively indicates the observed and the map VTEC for 2, 4, 6,8,10,12,14,16 and 18 UTCs. The 2^{nd},3^{rd} , and 4^{th} columns, from the left, in these figures show the VTEC maps obtained from quadratic polynomial, NTCM driven by Az maps and daily F10.7, respectively. As seen in both figures, spatial variations of observed VTEC (left panels) are

similar with the spatial variations of VTEC maps obtained from polynomial and NTCM driven by Az maps compared to VTEC maps of NTCM driven by F10.7. More importantly , the equatorial ionization anomaly (EIA) shown by observations are captured by the VTEC maps obtained by polynomial fit and NTCM after adaptation; whereas the NTCM map of VTEC before adaptation (right column) portrayed smooth latitude variations of VTEC that don't agree with observations. These plots also show that polynomial fit and NTCM driven by Az map captures the diurnal variation of VTEC maps much better than the NTCM model driven its standard input (F10.7). Therefore, the model VTEC after adaptation is in good agreement with the experimental VTEC as compared to model VTEC before adaptation. This means that the local ionization level, Az drives NTCM model by far better than the solar flux, F10.7.

Conclusion

Data ingestion into NTCM model has been carried out to validate the performance of the model in estimating VTEC of the East-African Ionosphere sector. This has been done by determining the optimum value of the input effective ionization level Az and by running the model using Az. We found that data ingestion into NTCM enables it to estimate diurnal observed TEC in a better way than it estimates before ingestion. The model driven by Az's of a reference station, in regions around it, estimates the observed VTEC better than the model driven by F10.7. After adaptation the mismodeling means and standard deviations have significantly decreased in comparison to the mismodeling means and standard deviations before adaptation. This reduction of means and standard deviations quantifies the improvement of the performance of the model after ingestion. The model driven by Az computed at 1hr ahead can estimate the measured VTEC better than it is driven by Az computed at 4 hrs ahead. Moreover, NTCM VTEC maps reproduced from updated Az maps by polynomial fitting reflect the VTEC maps developed by polynomial fitting of the observed VTEC including the EIA which are not seen by the NTCM VTEC maps using the standard input F10.7. These findings suggest that the proposed ingestion technique can bring a performance improvement to NTCM model and it is effective to progress from climatology model to a model that describes the near-real-time weather conditions of the ionosphere.

Acknowledgments: The authors would like to thank the UNAVCO Consortium for GPS data freely available at https://www.unavco.org/ and NASA for F10.7 data available at https://omniweb.gsfc.nasa.gov/form/dx1.html.The work has been partially supported by Air

Force Office of Scientific Research and Air Force Office of Material Command USAF under Award FA9550-16-1-0070. The authors are also grateful to Norbert Jakowiski and Mainul Hoque for the code of the NTCM model we used.

References

Angling, M. J., & N.K. Jackson –Booth (2011), A short note on the assimilation of collocated and concurrent GPS and ionosonde data into the Electron Density Assimilative Model, *Radio Sci.*,doi:10.1029/2010RS004566.

Bilitza, D., & Reinisch, B. W. (2008), International reference ionosphere 2007: Improvements and new parameters, *Advances in Space Research*, 42, 599– 609, doi : 10.1016/j.asr.2007.07.048.

Bilitza, D., Altadill, D., Truhlik, V., Shubin, V., Galkin, I., Reinisch, B., and Huang, X. (2017): International Reference Ionosphere 2016: From ionospheric climate to real-time weather predictions, Space Weather, 15, 418–429, DOI: 10.1002/2016SW001593

Brunini, C., Azpilicueta,F., Gende ,M. Camilion, E., Aragón-Ángel, A. Hernandez-Pajares ,M. , Juan ,M., Sanz ,J., Dagoberto Salazar (2011), Ground- and space-based GPS data ingestion into the NeQuick model, *J.Geod.,* doi: 10.1007/s00190-011-0452-4.

Ciraolo, L., F. Azpilicueta, C. Brunini, A. Meza, and S. M. Radicella (2007), Calibration errors on experimental slant total electron content (TEC) determined with GPS, *J. Geod., 81, 111–120.*

Davies, K. (1990), Ionosphere Radio, *Peter Peregrinus Ltd., London*, doi:10.1049/PBEW031E.

Deminov M. G. and Deminova G.F (2018), Solar Activity for Long-Term Prediction of the F2 Layer Critical Frequency , Geomagnetism and Aeronomiya , DOI: 10.1134/S0016793219020063.

Ercha Aa, Aaron Ridley, Wengeng Huang, Shasha Zou, Siqing Liu, Anthea J. Coster, and Shunrong Zhang (2018), An Ionosphere Specification Technique Based on Data Ingestion Algorithm and Empirical Orthogonal Function Analysis Method, *American Geophysical Union*, doi: 10.1029/2018SW001987.

Jakowski, N., M. M. Hoque and C. Mayer (2011), A new global TEC model for estimating transionospheric radio wave propagation errors , J.Geod., doi :10.1007/s00190-011-0455-1.

Mannucci, A. J., B. D. Wilson, D. N. Yuan, C. H. Ho, U. J. Lindqwister, and T. F. Runge (1998), A global mapping technique for GPS-derived ionospheric total electron content measurements, *Radio Sci., 33, 565–582*, doi:10.1029/97RS02707.

Nava, B., S. M. Radicella, R. Leitinger, and P. Coïsson (2006), A near real-time model-assisted ionosphere electron density retrieval method, *Radio Sci., 41, RS6S16*, doi: 10.1029/2005RS003386.

Nava, B., P. Coïsson, and S. M. Radicella (2008), A new version of the NeQuick ionosphere electron density model, J. Atmos. Sol. Terr. Phys., 70, 1856–1862, doi:10.1016/j.jastp.2008.01.015.

Nava, B., Radicella, S. M., & Azpilicueta, F. (2011), Data ingestion into NeQuick 2, *Radio Science, 46, RS0D17*, doi: 1029/2010RS004635.

Nigussie, M., S. M. Radicella, B. Damtie, B. Nava, E. Yizengaw, and L. Ciraolo (2012), TEC ingestion into NeQuick 2 to model the East African equatorial ionosphere, *Radio Sci., 47, RS5002*, doi:10.1029/2012RS004981.

Nigussie, M., Radicella,S. M., Damtie, B., Yizengaw, E. , Nava, B. and Roininen, L.(2016), Validation of NeQuick TEC data ingestion technique against C/NOFS and EISCAT electron density measurements, *Radio Sci.,* doi:10.1002/2015RS005930.

Olwendo, O.J., Cesaroni, C. (2016), Validation of NeQuick 2 model over the Kenyan region through data ingestion and the model application in ionospheric studies, *J.Atmo.and Solar-T. physics*.

Rawer, K.(1993), Wave Propagation in the Ionosphere, *Kluwer Acad.Publ, Dordrechet.*

Scherliess, L., D. Thompson, and R. W. Schunk (2008), Longitudinal variability of low-latitude total electron content: Tidal influences, *J. Geophys. Res., 113, A01311*, doi: 10.1029/2007JA012480.

Schunk, R., Nagy, R. (2009), Ionospheres – Physics, Plasma Physics, and Chemistry, *Cambridge University Press, Physics.*

Schunk, R. W., et al. (2004), Global Assimilation of Ionospheric Measurements (GAIM*), Radio Sci., 39, RS1S02*, doi:10.1029/2002RS002794.

Tariku,Y. (2015), TEC prediction performance of the IRI-2012 model over Ethiopia during the rising phase of solar cycle 24 (2009–2011), *Earth, planets and Space,* doi; 0.1186/s40623-015-0312-1.

Tiwari, R., Strangeways, H.J., Tiwari, S., Ahemad, A.(2013), Investigation of ionospheric irregularities and scintillation using TEC in highlatitude, *Adv. Space Res. 52, 1111–1124.*

Wang, C., G. Hajj, X. Pi, I. G. Rosen, and B. Wilson (2004), Development of the Global Assimilative Ionospheric Model, *Radio Sci., 39, RS1S06*, doi:10.1029/2002RS002854.

Zolesi B· Cander L.R., 2014, Ionospheric Prediction and Forecasting, *Springer Heidelberg New York Dordrecht London*, doi: 10.1007/978-3-642-38430-1.

Figure 1: Diurnal variation of experimental and modeled (before & after data ingestion) VTEC (left); frequency distribution of mismodeling of VTEC after (middle), and before (right) data ingestion at Ambo station for DOY 79,171,263 and 355 in 2014.

Figure 2: Diurnal variation of experimental and modeled (before & after data ingestion) VTEC (left); frequency distribution of mismodeling of VTEC after (middle), and before (right) data ingestion at Bahir Dar station for DOY 79,171,263 and 355 in 2014.

Figure 3: Diurnal variation of experimental and modeled (before & after data ingestion) VTEC (left); frequency distribution of mismodeling of VTEC after (middle), and before (right) data ingestion at Addis Ababa station for DOY 79,171,263 and 355 in 2014.

Figure 4: Diurnal variation of experimental and modeled (before & after data ingestion) VTEC (left); frequency distribution of mismodeling of VTEC after (middle), and before (right) data ingestion at Malindi station for DOY 79,171,263 and 355 in 2014.

Figure 5: Diurnal variation of experimental and modeled (before & after data ingestion) VTEC (left); frequency distribution of mismodeling of VTEC after (middle), and before (right) data ingestion at Mbarara station for DOY 79,171,263 and 355 in 2014.

Figure 6: Diurnal variation of experimental and modeled (before & after data ingestion) VTEC (left); frequency distribution of mismodeling of VTEC after (middle), and before (right) data ingestion at Assab station for DOY 79,171,263 and 355 in 2014.

Figure 7: Frequency distribution of VTEC mismodeling after (left) and before (right) ingestion for 354 quiet days in 2014 at Ambo station.

Figure 8: Diurnal variation of experimental and modeled (using F10.7 & Az computed at Addis Ababa) VTEC (left); frequency distribution of mismodeling of VTEC using F10.7 (middle), and Az (right) at Ambo station for DOY 79,171,263 and 355 in 2014.

Figure 9: Diurnal variation of experimental and modeled (using F10.7 & Az computed at Addis Ababa) VTEC (left); frequency distribution of mismodeling of VTEC using F10.7 (middle), and Az (right) at Bahir Dar station for DOY 79,171,263 and 355 in 2014.

Figure 10: Diurnal variation of experimental and modeled (using F10.7 & Az computed at Addis Ababa) VTEC (left); frequency distribution of mismodeling of VTEC using F10.7 (middle), and Az (right) at Assab station for DOY 79,171,263 and 355 in 2014.

Figure 11: Diurnal variation of experimental and modeled (using F10.7 & Az computed at Addis Ababa) VTEC (left); frequency distribution of mismodeling of VTEC using F10.7 (middle), and Az (right) at Nazret station for DOY 79,171,263 and 355 in 2014.

Figure 12: Diurnal variation of experimental modeled (before & after data ingestion) and predicted VTEC at Ambo station for DOY 355 in 2014. Panels a,b,c and d are 1hr,2hrs,3hrs and 4hrs time of prediction respectively.

Figure 13: Scatter plot of experimental VTEC versus latitude and longitude , from top to bottom at 2,4,6,8 & 10 UT (left) , and the corresponding VTEC map from polynomial function (2^{nd} column from left), NTCM derived by Az map (3^{rd} column from left) and F10.7(4^{th} column from left) on DOY 110 of 2013.

Figure 14: Scatter plot of experimental VTEC versus latitude and longitude , from top to bottom at 12,14,16 & 18 UT (left) , and the corresponding VTEC map from polynomial function (2^{nd} column from left), NTCM derived by Az map (3^{rd} column from left) and by F10.7(4^{th} column from left) on DOY 110 of 2013.

Figure 1.

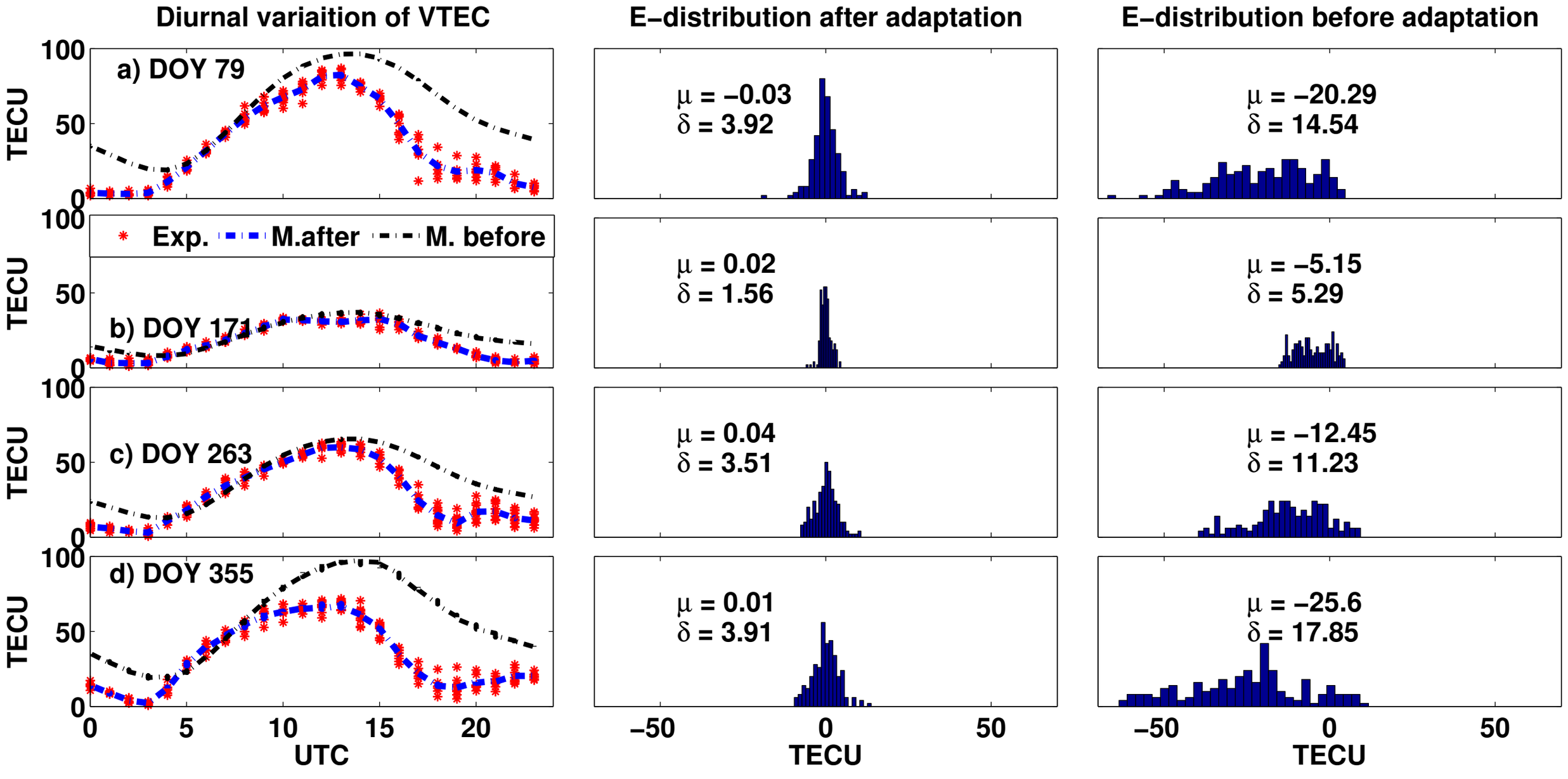
Diurnal variaition of VTEC
E–distribution after adaptation
E–distribution before adaptation
a) DOY 79
b) DOY 171
c) DOY 263
d) DOY 355
Exp.
M.after
M. before
TECU
UTC
μ = –0.03
δ = 3.92
μ = 0.02
δ = 1.56
μ = 0.04
δ = 3.51
μ = 0.01
δ = 3.91
μ = –20.29
δ = 14.54
μ = –5.15
δ = 5.29
μ = –12.45
δ = 11.23
μ = –25.6
δ = 17.85

Figure 2.

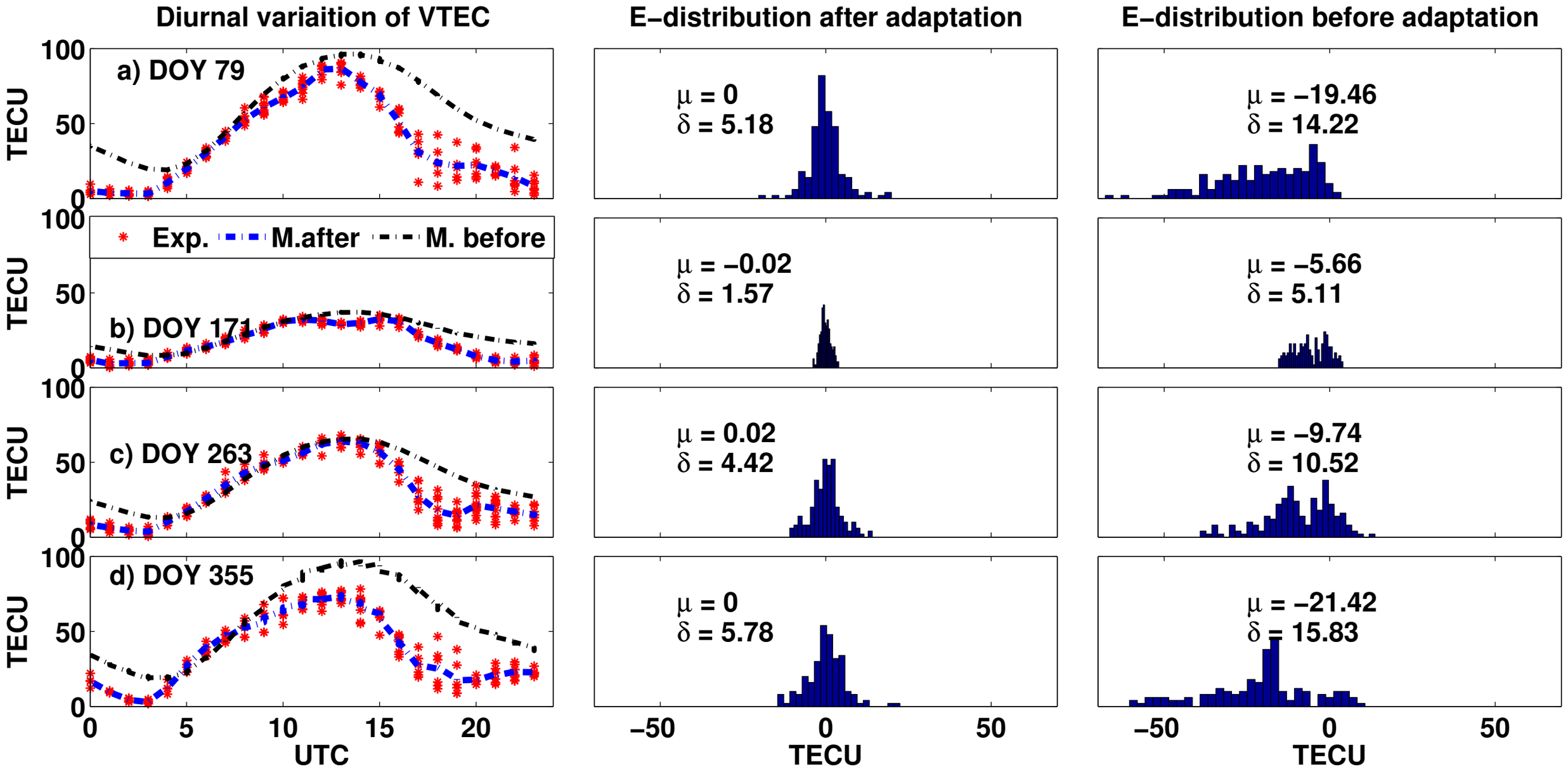
Diurnal variaition of VTEC
E–distribution after adaptation
E–distribution before adaptation
a) DOY 79
b) DOY 171
c) DOY 263
d) DOY 355
Exp.
M.after
M. before
TECU
UTC
μ = 0
δ = 5.18
μ = –19.46
δ = 14.22
μ = –0.02
δ = 1.57
μ = –5.66
δ = 5.11
μ = 0.02
δ = 4.42
μ = –9.74
δ = 10.52
μ = 0
δ = 5.78
μ = –21.42
δ = 15.83

Figure 3.

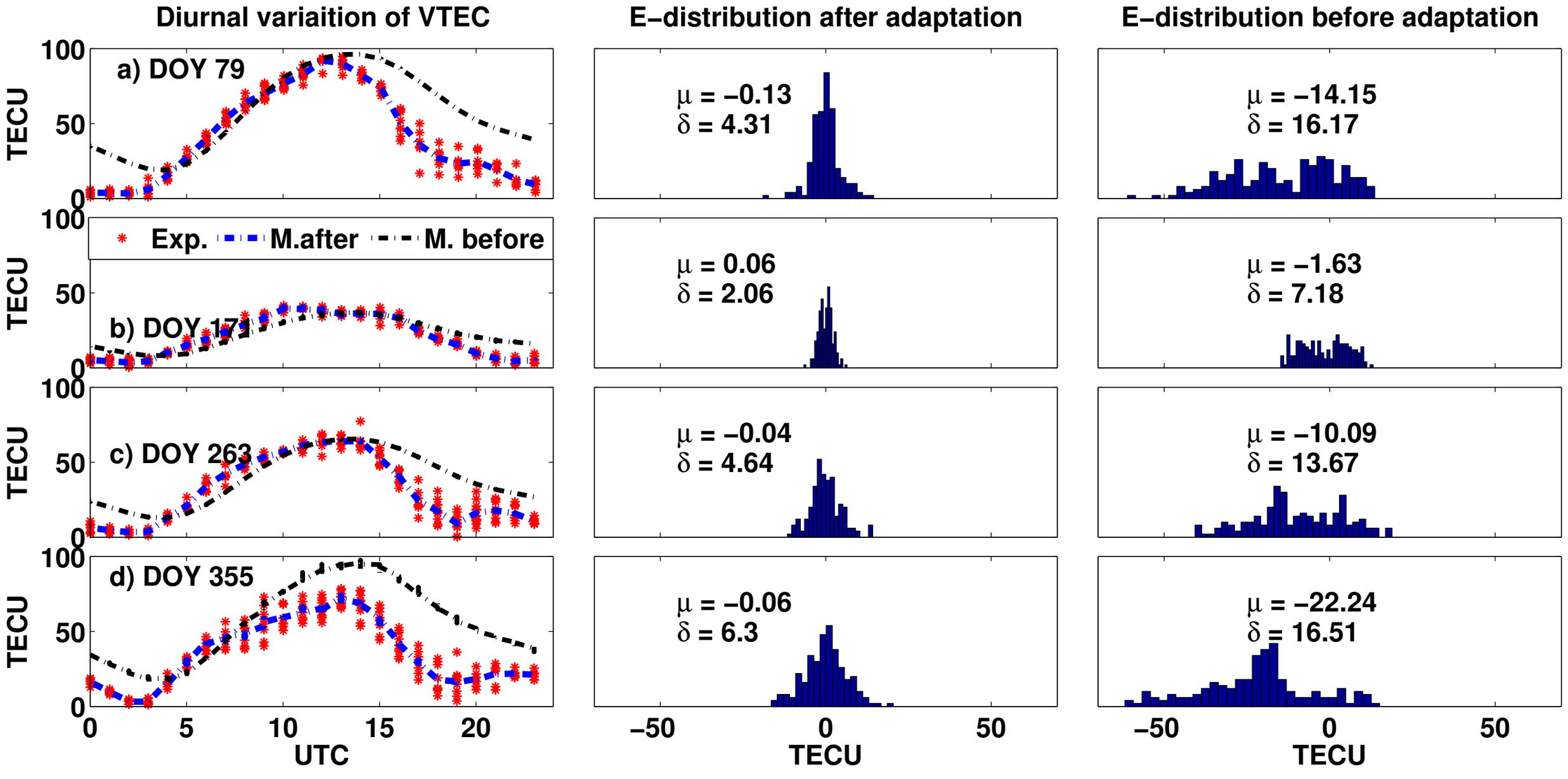
Diurnal variaition of VTEC
E–distribution after adaptation
E–distribution before adaptation
a) DOY 79
b) DOY 171
c) DOY 263
d) DOY 355
Exp.
M.after
M. before
TECU
UTC
μ = –0.13
δ = 4.31
μ = 0.06
δ = 2.06
μ = –0.04
δ = 4.64
μ = –0.06
δ = 6.3
μ = –14.15
δ = 16.17
μ = –1.63
δ = 7.18
μ = –10.09
δ = 13.67
μ = –22.24
δ = 16.51

Figure 4.

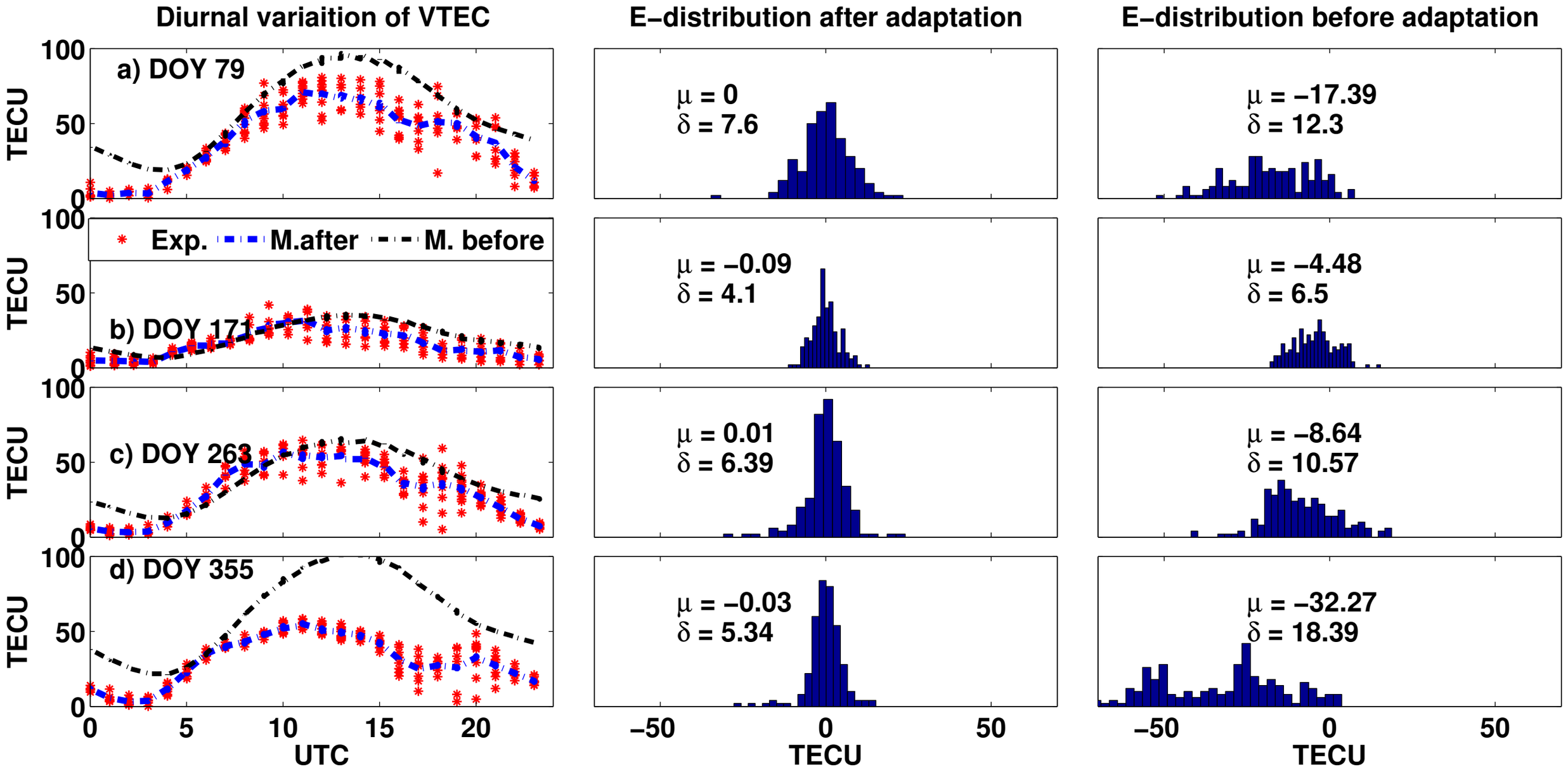
Diurnal variaition of VTEC
E–distribution after adaptation
E–distribution before adaptation
a) DOY 79
b) DOY 171
c) DOY 263
d) DOY 355
Exp.
M.after
M. before
TECU
UTC
μ = 0
δ = 7.6
μ = –17.39
δ = 12.3
μ = –0.09
δ = 4.1
μ = –4.48
δ = 6.5
μ = 0.01
δ = 6.39
μ = –8.64
δ = 10.57
μ = –0.03
δ = 5.34
μ = –32.27
δ = 18.39

Figure 5.

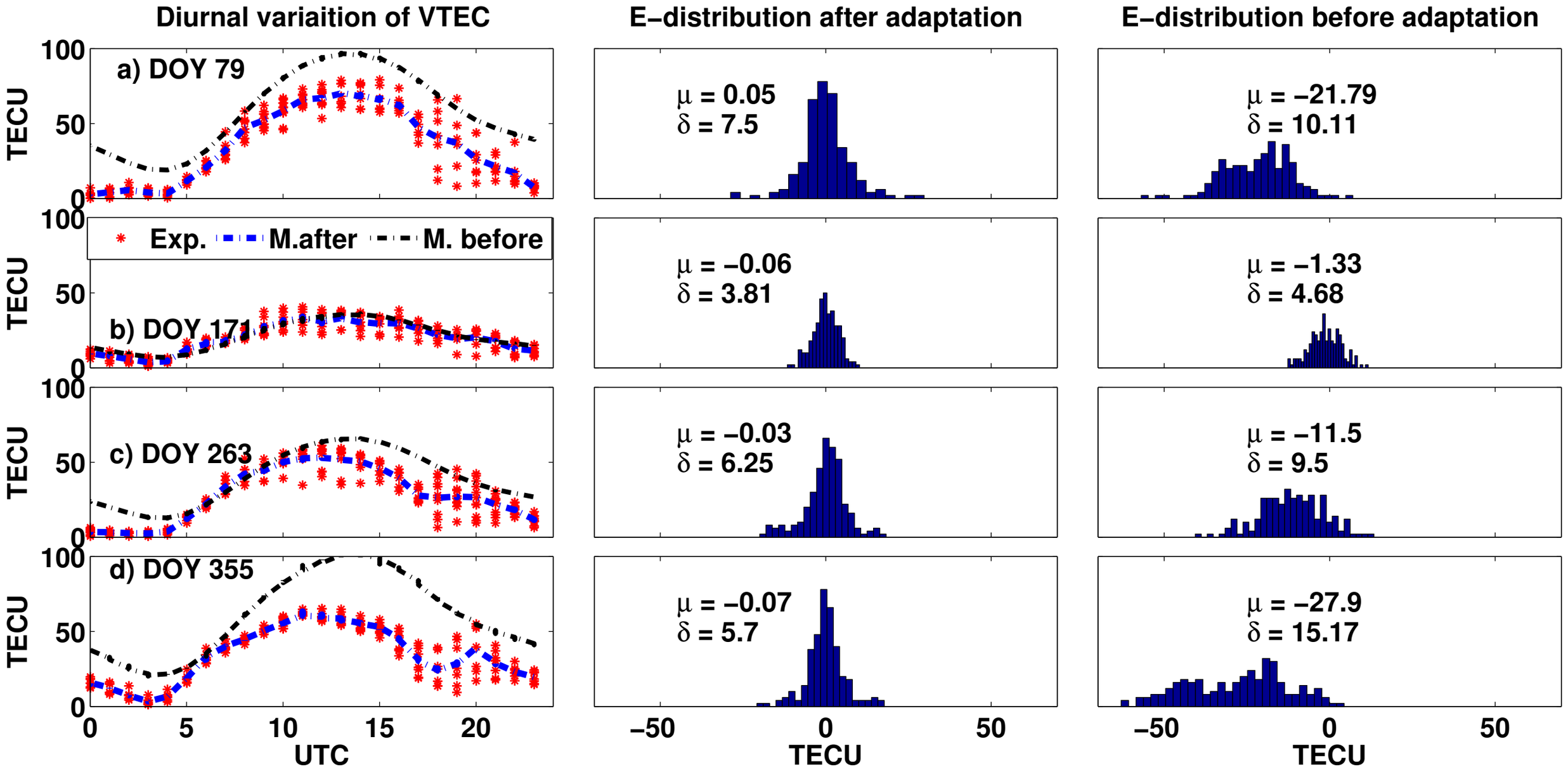
Diurnal variaition of VTEC
E–distribution after adaptation
E–distribution before adaptation
a) DOY 79
b) DOY 171
c) DOY 263
d) DOY 355
Exp.
M.after
M. before
TECU
UTC
μ = 0.05
δ = 7.5
μ = –21.79
δ = 10.11
μ = –0.06
δ = 3.81
μ = –1.33
δ = 4.68
μ = –0.03
δ = 6.25
μ = –11.5
δ = 9.5
μ = –0.07
δ = 5.7
μ = –27.9
δ = 15.17

Figure 6.

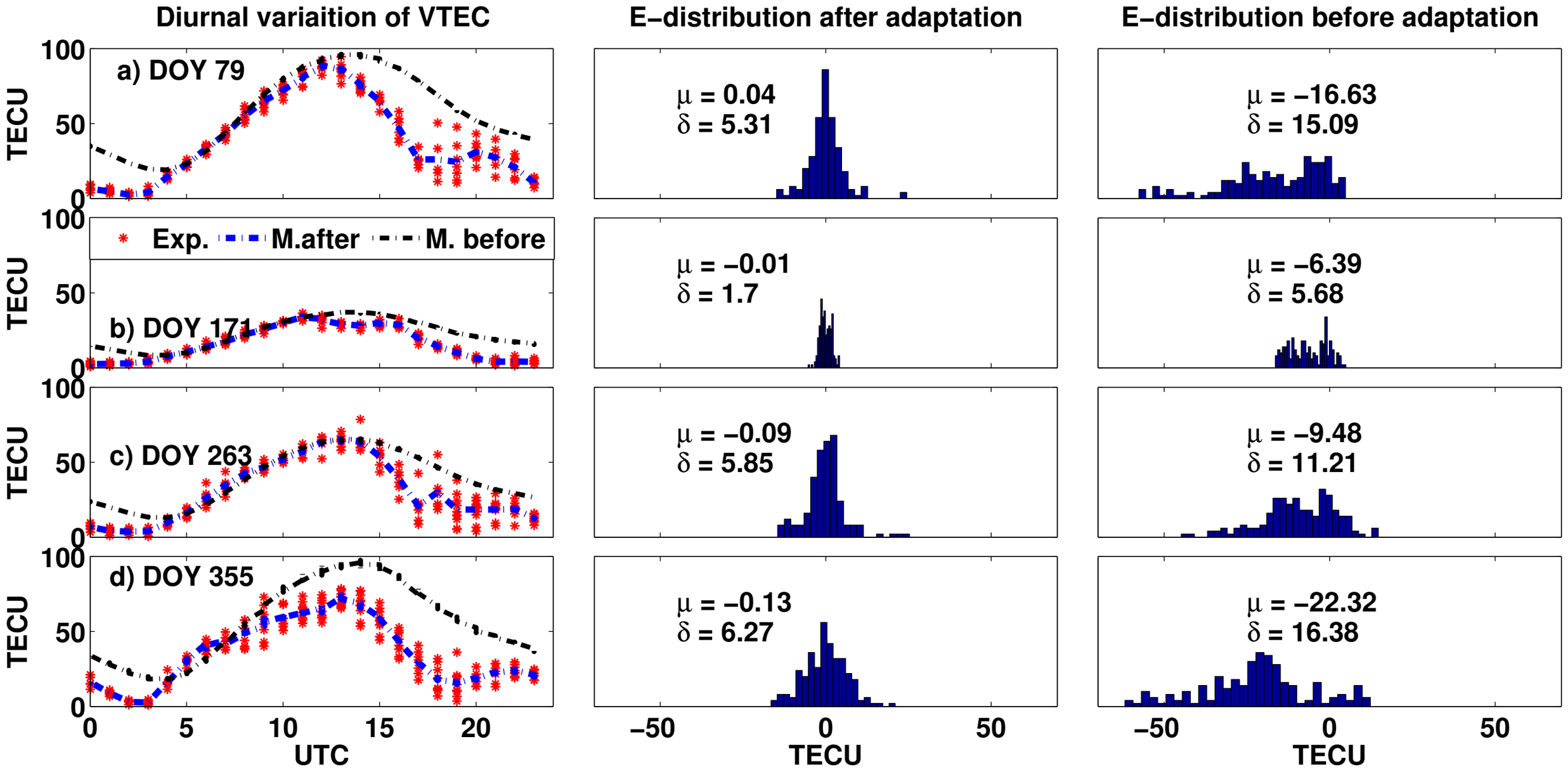
Diurnal variaition of VTEC
E−distribution after adaptation
E−distribution before adaptation
a) DOY 79
b) DOY 171
c) DOY 263
d) DOY 355
Exp.
M.after
M. before
TECU
UTC
μ = 0.04
δ = 5.31
μ = −16.63
δ = 15.09
μ = −0.01
δ = 1.7
μ = −6.39
δ = 5.68
μ = −0.09
δ = 5.85
μ = −9.48
δ = 11.21
μ = −0.13
δ = 6.27
μ = −22.32
δ = 16.38

Figure 7.

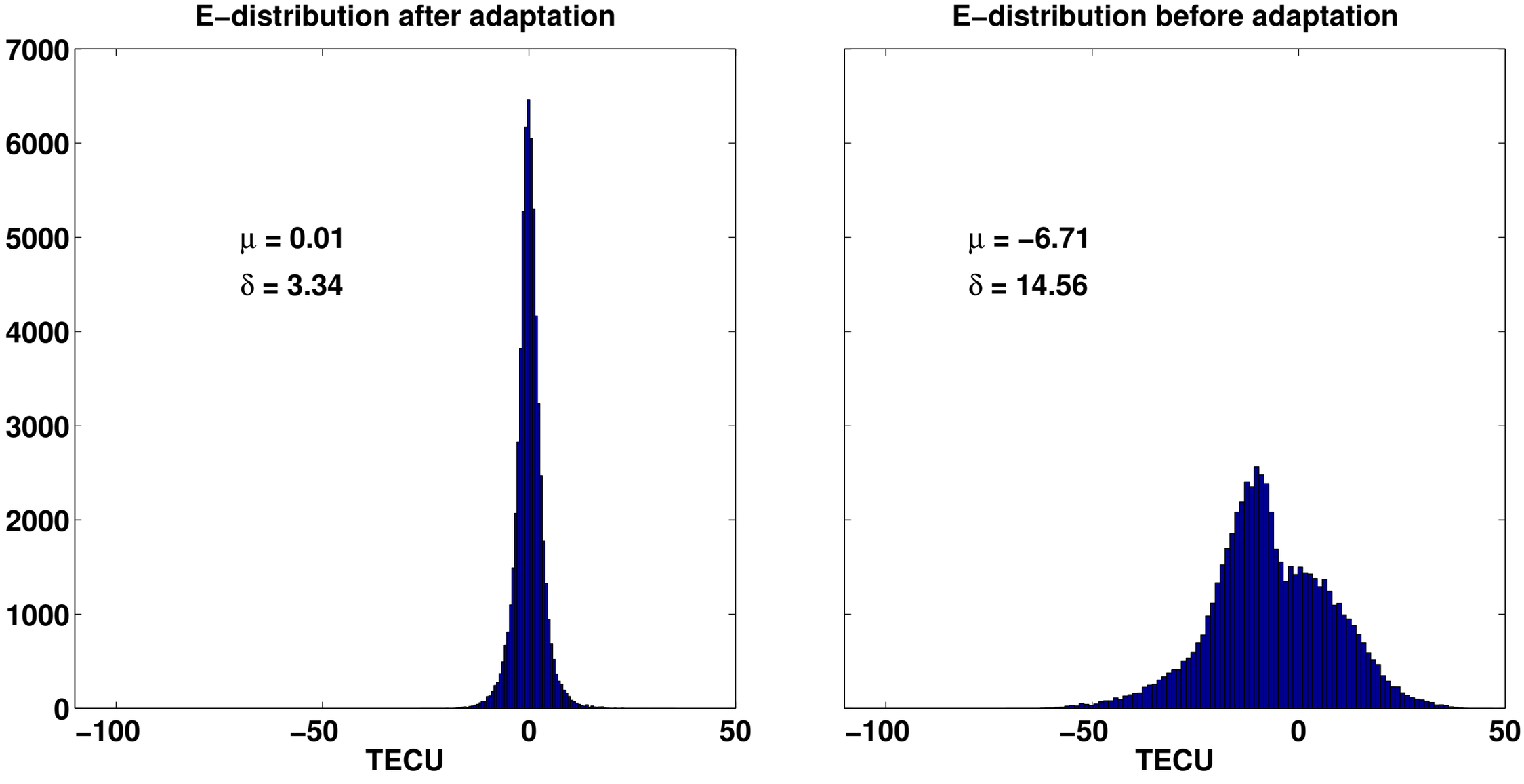
E–distribution after adaptation
μ = 0.01
δ = 3.34
7000
6000
5000
4000
3000
2000
1000
0
–100
–50
0
50
TECU
E–distribution before adaptation
μ = –6.71
δ = 14.56
–100
–50
0
50
TECU

Figure 8.

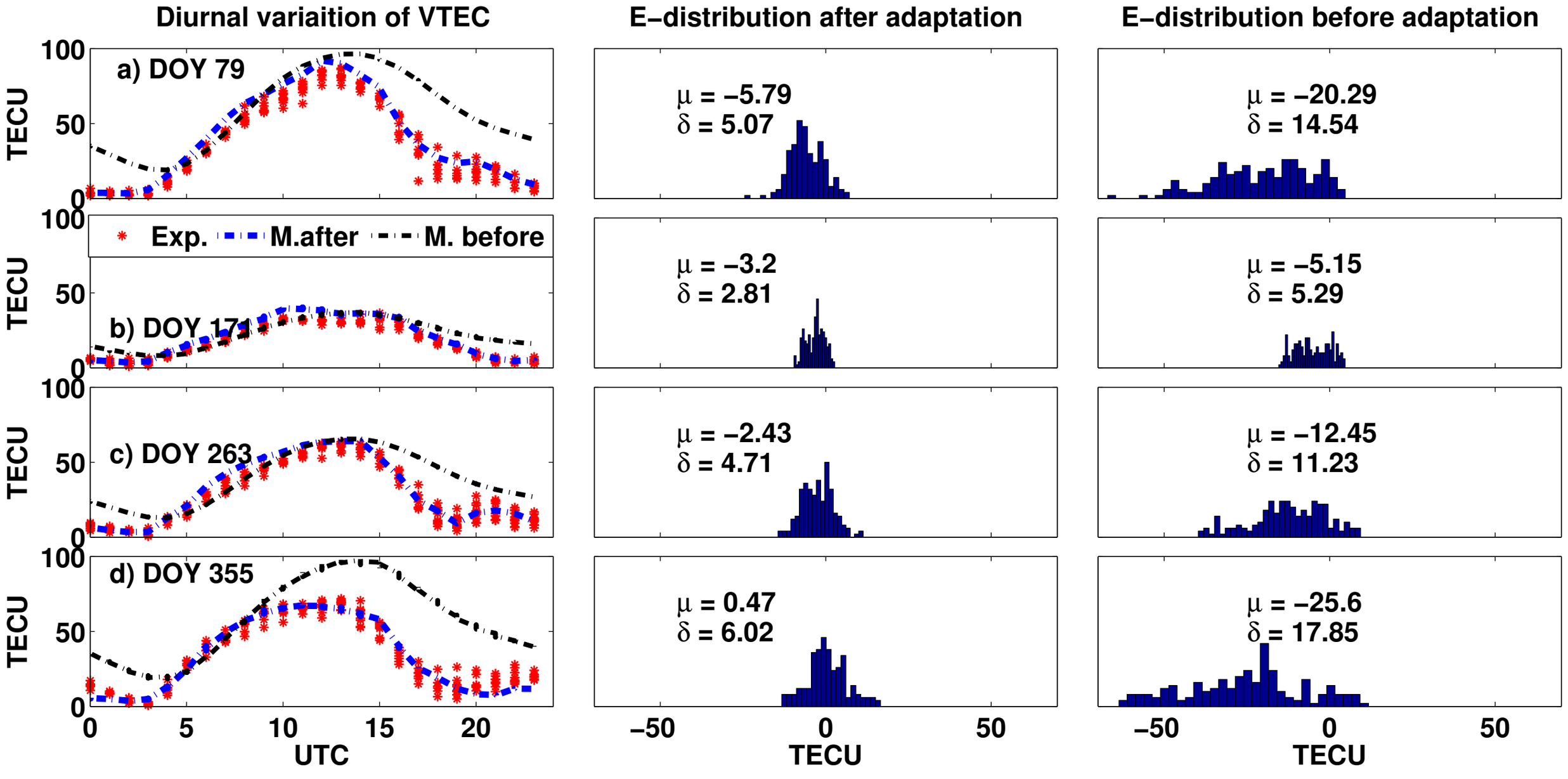
Diurnal variaition of VTEC
E–distribution after adaptation
E–distribution before adaptation
a) DOY 79
b) DOY 171
c) DOY 263
d) DOY 355
Exp.
M.after
M. before
TECU
UTC
μ = –5.79
δ = 5.07
μ = –20.29
δ = 14.54
μ = –3.2
δ = 2.81
μ = –5.15
δ = 5.29
μ = –2.43
δ = 4.71
μ = –12.45
δ = 11.23
μ = 0.47
δ = 6.02
μ = –25.6
δ = 17.85

Figure 9.

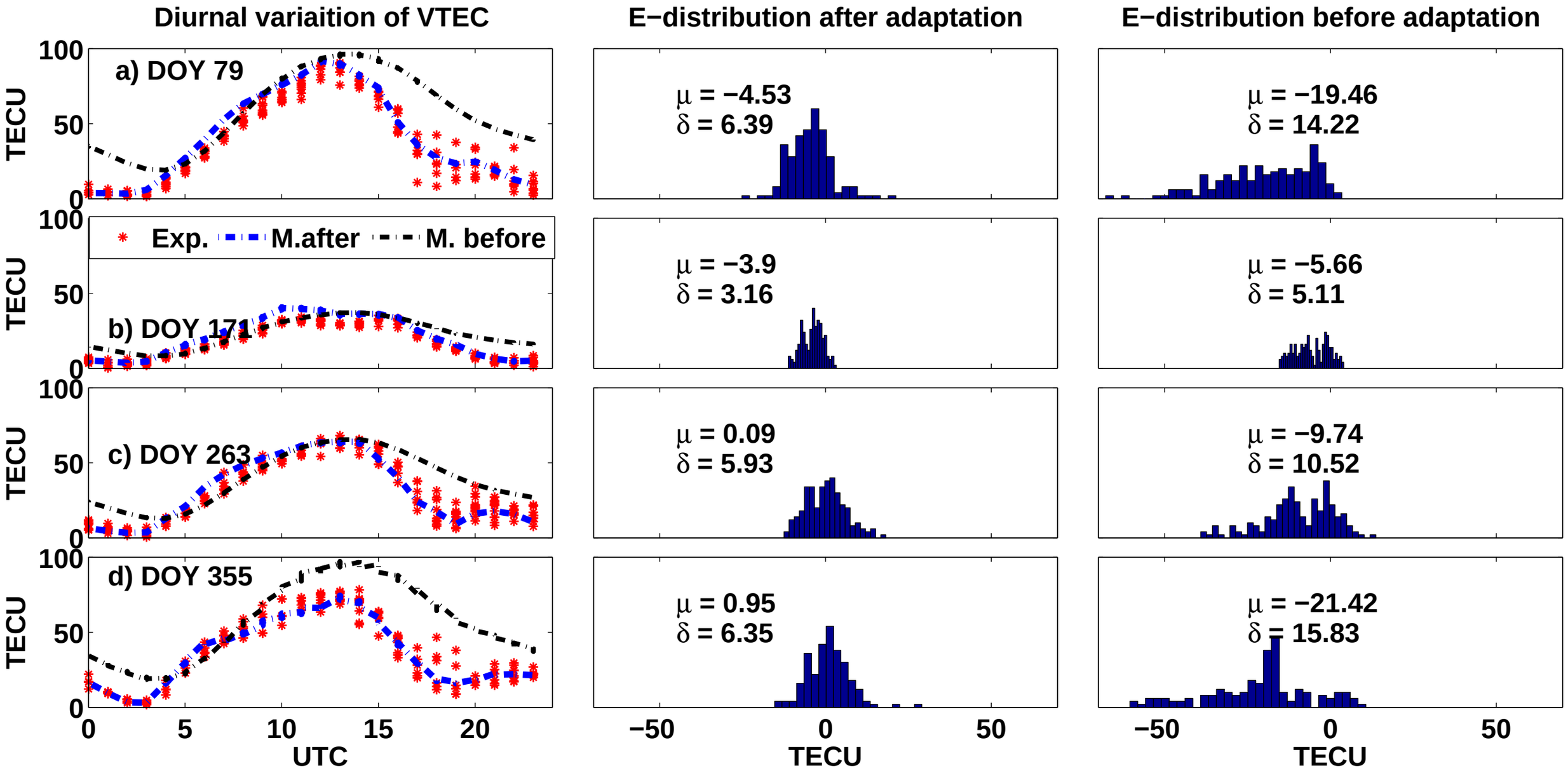
Diurnal variaition of VTEC
E−distribution after adaptation
E−distribution before adaptation
a) DOY 79
b) DOY 171
c) DOY 263
d) DOY 355
Exp.
M.after
M. before
TECU
UTC
μ = −4.53
δ = 6.39
μ = −19.46
δ = 14.22
μ = −3.9
δ = 3.16
μ = −5.66
δ = 5.11
μ = 0.09
δ = 5.93
μ = −9.74
δ = 10.52
μ = 0.95
δ = 6.35
μ = −21.42
δ = 15.83

Figure 10.

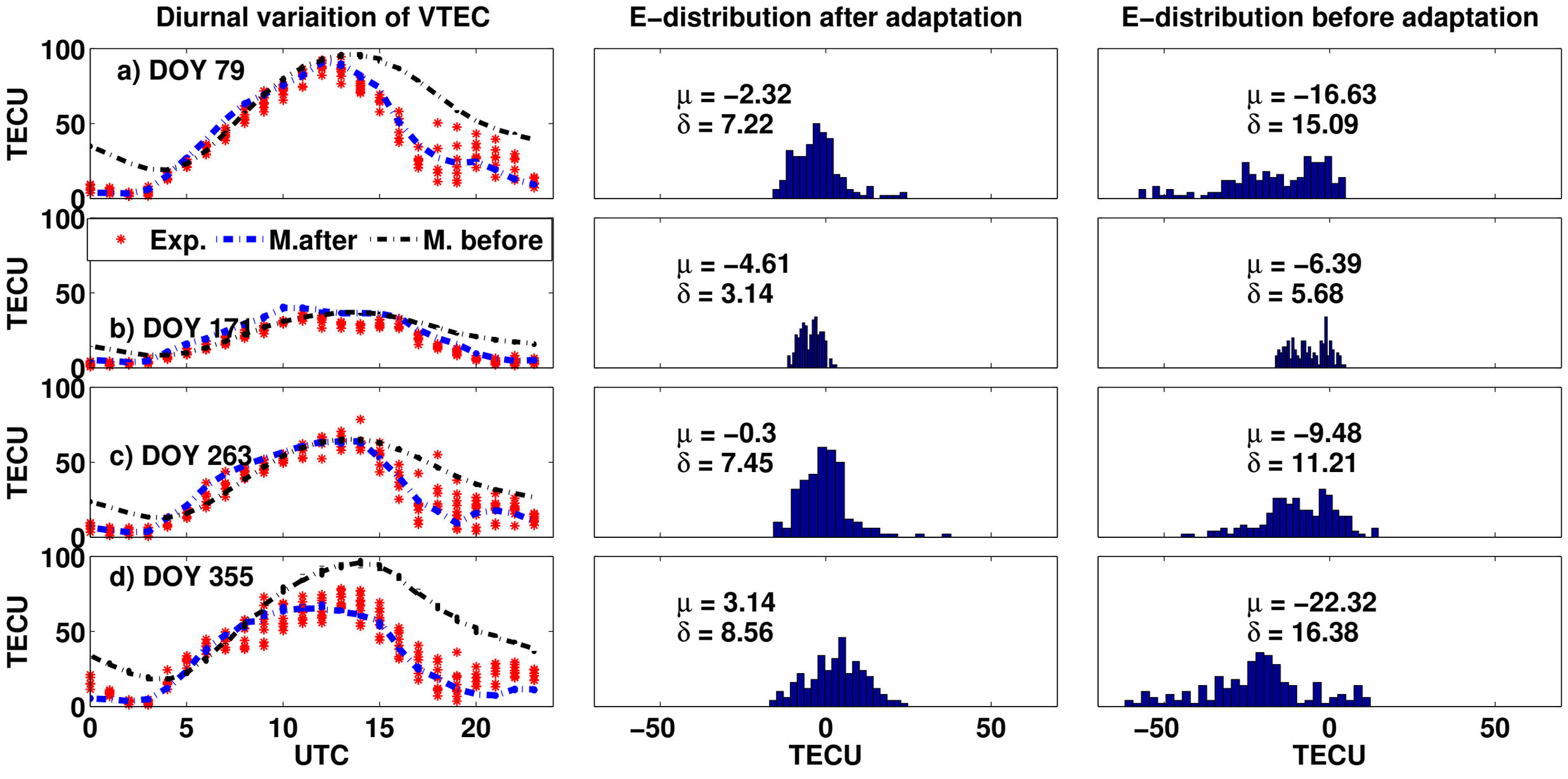
Diurnal variaition of VTEC
E−distribution after adaptation
E−distribution before adaptation
a) DOY 79
b) DOY 171
c) DOY 263
d) DOY 355
Exp.
M.after
M. before
TECU
UTC
μ = −2.32
δ = 7.22
μ = −16.63
δ = 15.09
μ = −4.61
δ = 3.14
μ = −6.39
δ = 5.68
μ = −0.3
δ = 7.45
μ = −9.48
δ = 11.21
μ = 3.14
δ = 8.56
μ = −22.32
δ = 16.38

Figure 11.

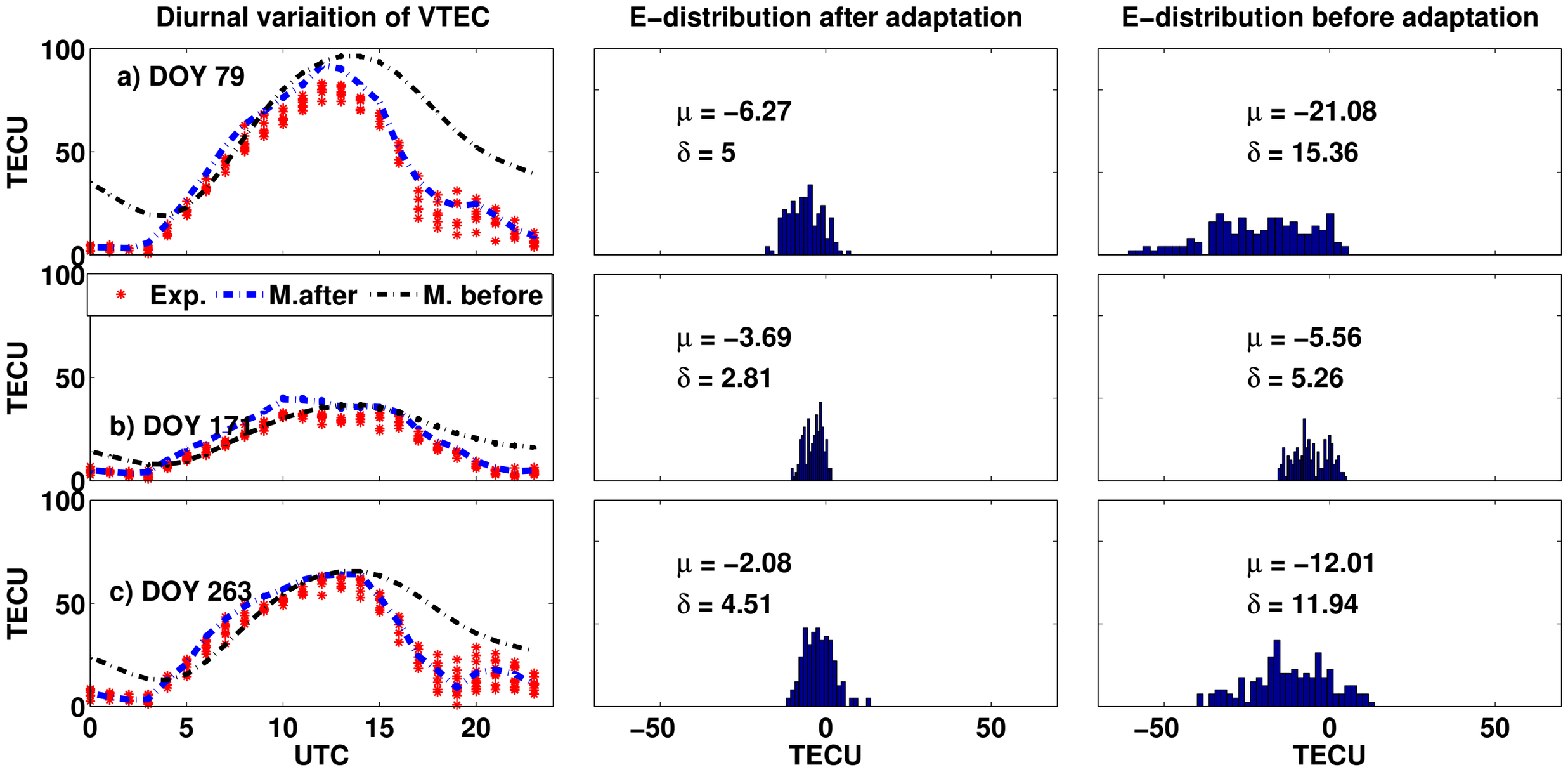
Diurnal variaition of VTEC
E–distribution after adaptation
E–distribution before adaptation
a) DOY 79
b) DOY 171
c) DOY 263
Exp.
M.after
M. before
TECU
UTC
μ = –6.27
δ = 5
μ = –21.08
δ = 15.36
μ = –3.69
δ = 2.81
μ = –5.56
δ = 5.26
μ = –2.08
δ = 4.51
μ = –12.01
δ = 11.94
0
50
100
0
5
10
15
20
–50
0
50

Figure 12.

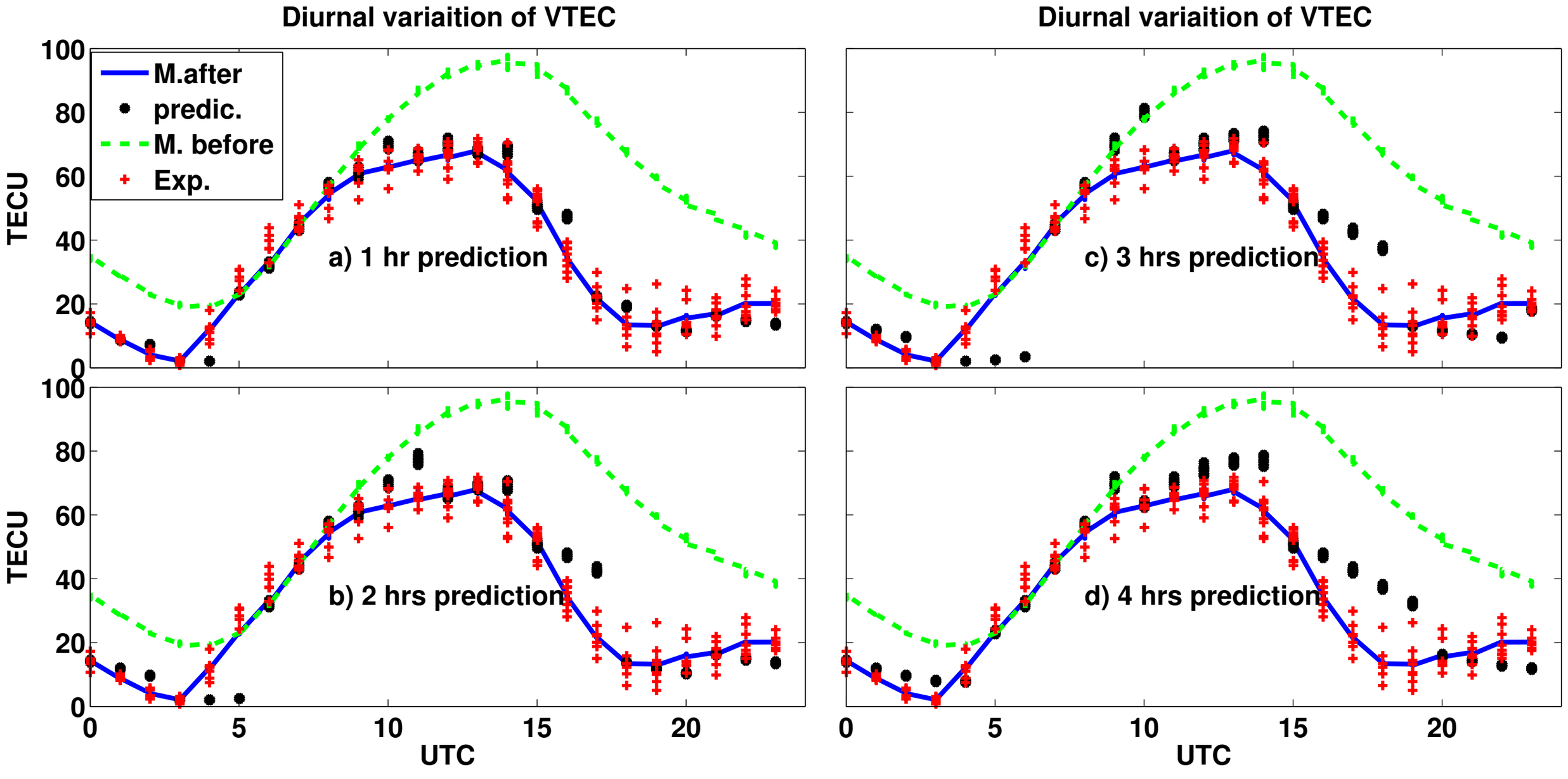
Diurnal variaition of VTEC
Diurnal variaition of VTEC
M.after
predic.
M. before
Exp.
a) 1 hr prediction
b) 2 hrs prediction
c) 3 hrs prediction
d) 4 hrs prediction
TECU
TECU
UTC
UTC
0
20
40
60
80
100
0
5
10
15
20

Figure 13.

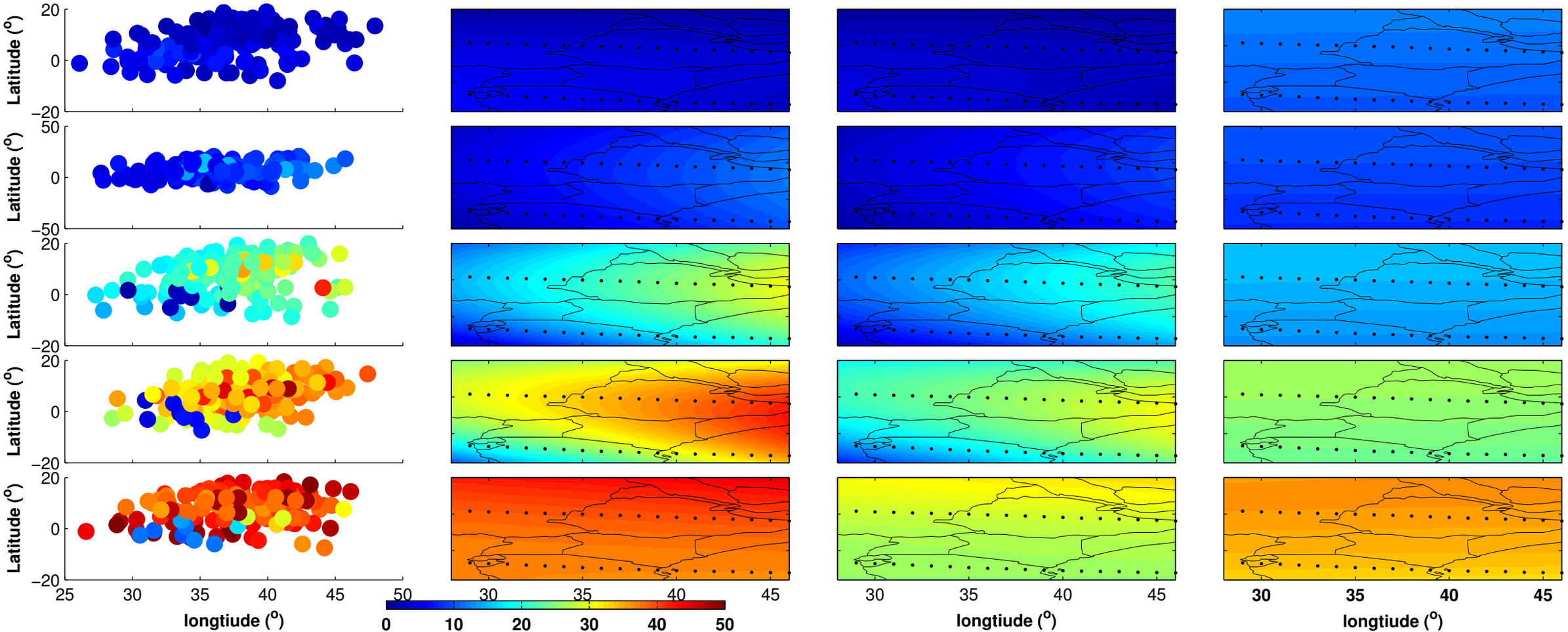
Latitude (°)
20
0
−20
50
−50
longtiude (°)
25
30
35
40
45
50
0
10
20
30
40
50

Figure 14.

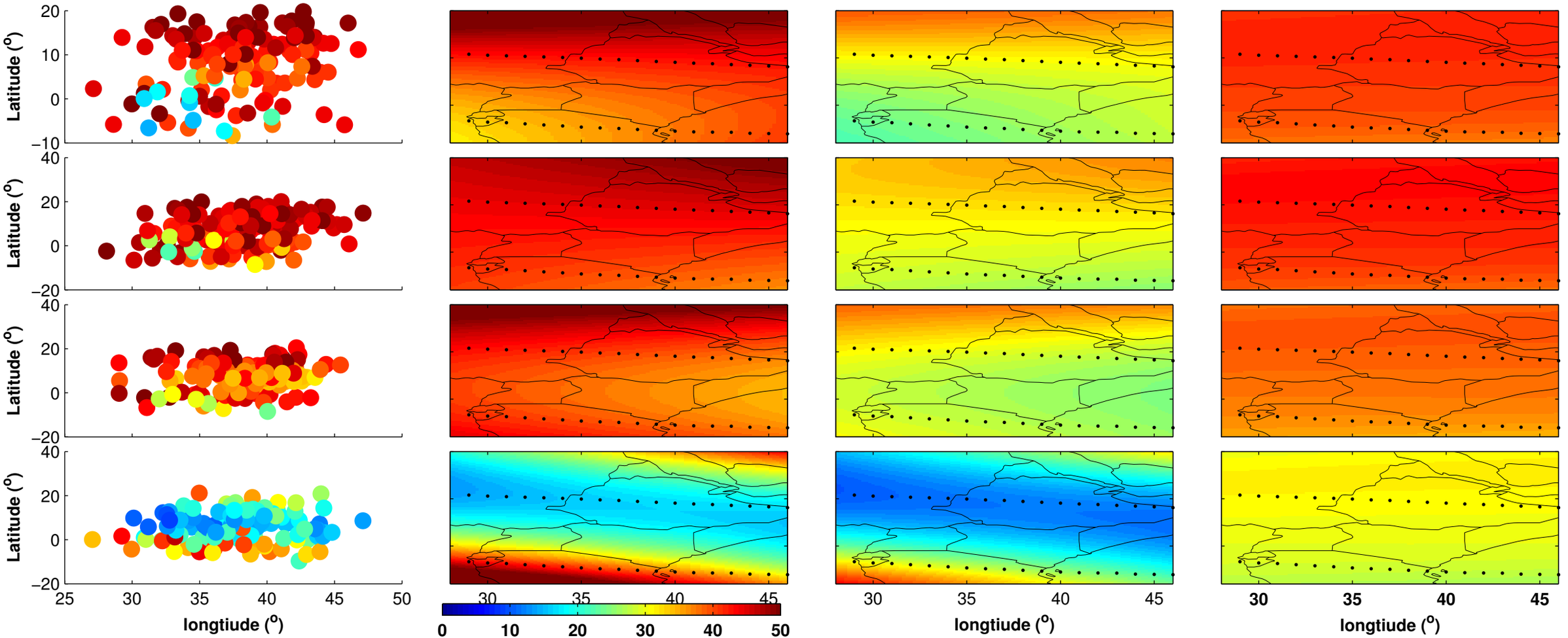
Latitude (°)
longtiude (°)
0
10
20
30
40
50